Int. J. Mech. Eng. & Rob. Res. 2014

International Journal of Mechanical Engineering and Robotics Research

ISSN 2278 – 0149 www.ijmerr.com
Vol. 3, No. 4, October 2014

Research Paper

FIELD TEST VALIDATION OF ANALYTICAL MODEL FOR VIBRATION CHARACTERISTICS OF A FLAP GATE UNDERGOING SELF-EXCITED VIBRATION

Keiko Anami[1]*, Noriaki Ishii[2], Charles W Knisely[3] and Yukio Matsumoto[4]

*Corresponding Author: Noriaki Ishii, ✉ ishii@isc.osakac.ac.jp

Experimental modal analysis, using an impact hammer and accelerometers, was conducted on a full-scale flap gate with a height of 0.963 m and a span of 14.8 m to determine its in-air natural frequencies, mode shapes, and modal damping. Subsequently, the in-water self-excited vibration characteristics of the gate (without any spoilers) were recorded using the same accelerometers. The major in-air vibration characteristics (the mode shape, frequency and damping ratio for the damped vibrations), as well as the major in-water self-excited vibration characteristics (the excitation ratio and frequency of the self-excited vibrations in-water) are tabulated. In parallel with these experiments, calculations of the inherent in-water vibration frequency of the gate using a potential flow theory, based on input from the in-air modal testing, are presented. Comparison of the calculated inherent in-water vibration frequency with the measured frequency of the in-water self-excited vibration confirms the validity of the present theoretical analysis.

Keywords: Flap gate, Flow-induced vibration, Added mass, Modal analysis, Self-excited vibration, In-water frequency

INTRODUCTION

Among the many hydraulic structures with which engineers deal, the hydraulic gate is one of great significance due to the volume of water it retains for flood protection, municipal water supply or irrigation purposes. The gate can be exposed to enormous hydraulic forces and is thus potentially subject to vibration. The loading

[1] Department of Mechanical Engineering, Ashikaga Institute of Technology, 268-1 Omae, Ashikaga, Tochigi 326-8558, Japan.
[2] Department of Mechanical Engineering, Osaka Electro-Communication University, Osaka, Japan.
[3] Department of Mechanical Engineering, Bucknell University, Lewisburg, PA 17837, USA.
[4] MeiwaConsulting Company, 474 Minami-mati, Nabari-city, Mie Prefecture 518-0729.

on the gate due to the inertia effects associated with the streamwise vibration of the gate can quickly lead to gate failure. The streamwise gate motion must also accelerate a tremendous mass of water in contact with the gate—the so-called added mass. This added mass also lowers the natural frequency of the gate and can lead to coalescence of initially disparate streamwise and vertical gate vibration frequencies. A case in point is the failure of the Folsom Dam Tainter gate in July 1995. Extensive investigations of this gate failure have been undertaken by Ishii (1995a, 1995b and 1997) and Anami and Ishii (1998a, 1998b, 1999, 2000 and 2003). Their results indicate that the hydrodynamic loading due to streamwise gate motion coupled with the vertical vibration of the gate most likely contributed to the failure.

It would be very useful to develop an analysis method, which would permit the calculation of the large magnitude hydrodynamic pressure acting on gate when it undergoes self-excited vibration. Ishii (1992), Ishii and Imaichi (1977), and Anami *et al.* (2012a and 2012b) developed an analysis method, which permits the calculation of these hydrodynamic pressures using potential theory for the dissipative wave radiation problem. Laboratory-scale model experiments (see Ishii, 1990, for example) have confirmed the analytical results. However, there has been no confirmation of these analytical predictions on a full-scale gate with overflow. An opportunity arose to undertake an experimental study of the vibration characteristics of a full-scale flap gate. The results were used to validate predictions made using the analytical method.

The field test was carried out on a flap gate, shown in Figure 1, with a height of 0.963 m, a span of 14.8 m and a mass of 3474 kg used to dam a river for irrigation purposes. The dam consisted of two such gates, located side-by-side with a center pier. By lowering the one

Figure 1: Cross-Sectional View of the Flap Gate in the River Installation

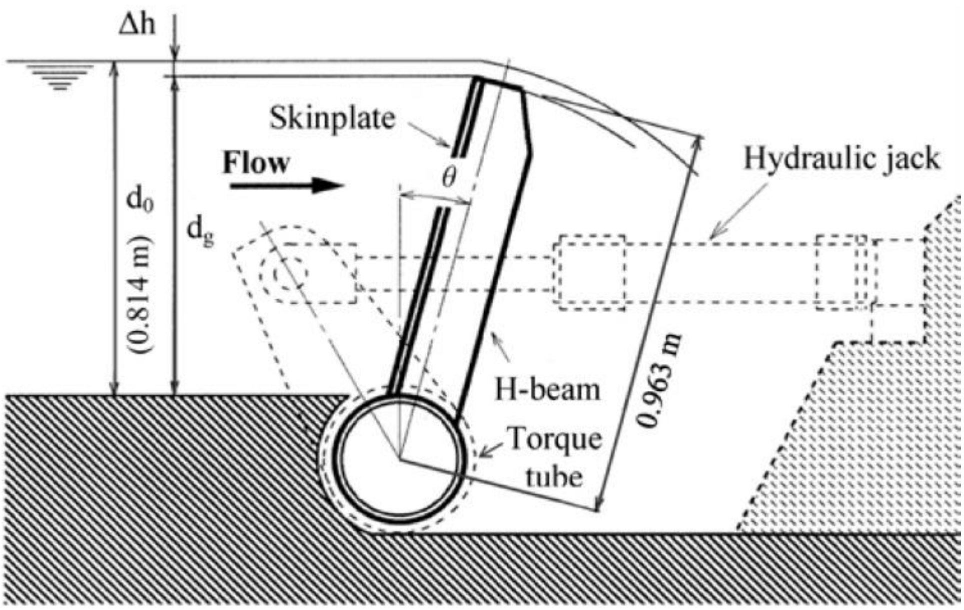

gate completely, the upstream reservoir was emptied and the other gate could be instrumented for in-air testing. The first series of tests were in-air experimental modal analyses, employing an impact hammer and accelerometers. The spanwise center of the gate was struck with a 5.4 kg impact hammer (PCB Model GK-086B50) and the vibrational acceleration response was measured at multiple locations on the gate surface using Lion LS-20C accelerometers.The accelerometer data was then processed using a digital computer to yield the modal frequencies, modal damping ratios and the mode shapes of the in-air natural vibration.

The second series of tests, those concerned with the in-water self-excited vibration of the gate, were conducted with the upstream reservoir restored and with water flowing over the instrumented test gate. For these tests, the spoilers that had been added to the gate crest to prevent vibration were removed. The flap gate quickly became unstable and experienced intense self-excited vibration. The accelerometers produced real-time records of the growth of these of self-excited vibrations. These real-time waveforms could then be processed to yield the frequency of vibration and the excitation ratio (the negative of the damping ratio).

Thirdly, since the lowest frequency natural vibration mode in air corresponds to the self-excited in-water mode, an analysis of the hydrodynamic pressure was carried out for this mode. The frequency of self-excitation in water was calculated from the equation of motion for the gate. Finally, the ratio of the frequency of self-excited vibration in water to the frequency of the in-air natural vibration was calculated both theoretically and from the experimental data. The comparison was made to confirm the validity of the present theoretical analysis.

MATERIALS AND METHODS

Detailed Flap Gate Description and Instrumentation

A sectional view of the full-scale flap gate is shown in Figure 1. The skinplate is rigidly attached to the torque tube. The skinplate thickness is 9 mm, and the radius of the torque tube is 156 mm. The distance from the torque tube center to top of the skinplate 0.963 m. The skinplate is reinforced by H-beams, 194 mm in height. The whole gate can be rotated around the torque tube by the hydraulic jack shown as a dashed line in Figure 1. The inclination angle of the gate relative to the vertical direction, denoted by ¯ in Figure 1, could be varied from 15º to 90º.

In the upstream view of the flap gate, shown in Figure 2, the span of the gate is given as 14.8 m. Also evident are the twelve H-beams reinforcing the skinplate. Figure 2 also shows many spoilers that were installed along the gate crest to attenuate self-excited vibration. These spoilers were removed during testing of the in-water self-excited vibrations. Unfortunately, they were not removed until after the in-air modal analysis, requiring a scaling of measured natural frequencies.

The natural vibration characteristics of the gate were determined by in-air experimental modal analysis, employing an impact hammer and accelerometers. With the upstream reservoir emptied, the gate was struck with a 5.4 kg impact hammer (PCB GK-086B50) which was instrumented with a force transducer (PCB GK-206M06). The location

Figure 2: Downstream View of Flap Gate Showing Impact Location and Accelerometer Locations for In-Air Modal Response and Self-Excited Acceleration Measurement

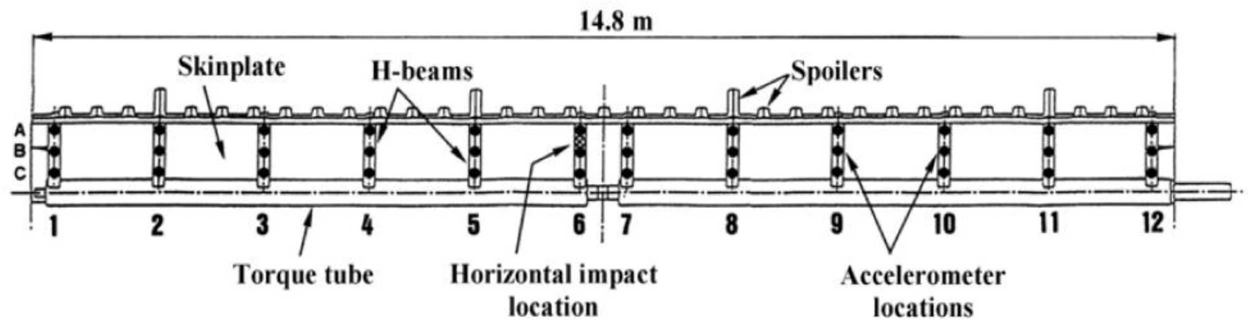

of the blow was chosen near the spanwise center as indicated by the ⊗ mark in Figure 2. The impact was in the upstream direction. The resultant acceleration response was measured by 6 servo-type mechanical accelerometers (Lion LS-20C). These 6 transducers were sequentially positioned at the 36 points indicated by the small black circles on the H-beams in Figure 2. For later reference, these points are denoted by a letter and a number according to the following scheme: A, B, C in order descending from the top and spanwise locations 1, 2, ..., 12 starting from the left side in Figure 2. The impact hammer force and the acceleration responses were recorded using a digital data recorder (TEAC RD-135D).

All data were analyzed on an FFT analyzer (A and D AD3525). Measured impulsive force and the resulting acceleration response at Point 6C are shown in Figures 3a and 3b.The acceleration power spectra were divided by the impulsive force power spectrum, resulting in the transfer functions at Point 6C, as shown in Figure 3c. This transfer function is the average of 3 sets of impact and response data.

The calculated transfer functions for all 36 measurement points were input into a modal analysis software package (AD1461 by Zonic Co.). The software package calculated and displayed the Inverse Modal Indicator Functions (IMIF) shown in Figure 4, which is defined by the following expression:

$$IMIF \equiv 1.0 - \frac{\sum_{i=1}^{n}\left[\left|Real\left(T_i\right)\right| \times \left|T_i\right|\right]}{\sum_{i=1}^{n}\left|T_i\right|^2} \quad ...(1)$$

where T_i represents a transfer function. The second term of Equation (1) corresponds to cos¤, where ¤ is the phase-lag of the vibration response relative to the excitation force and takes a value of 90° for resonance. Therefore, the peaks of the IMIF show a level of intensity at potential natural frequencies of the gate. The frequencies of the IMIF peaks were selected and the software attempted to calculate corresponding mode shapes. All peaks do not necessarily result in reasonable mode shapes. However, a fair number of the IMIF peaks resulted in meaningful mode shapes. The peaks corresponding to these modes are marked in Figure 3c for the transfer function and Figure 4 for the IMIF.

Figure 3: Sample of Measured Data Showing (a) The Impulsive Impact Force, (b) The Acceleration Response at Point 6C, and (c) The Transfer Functions for Point 6C

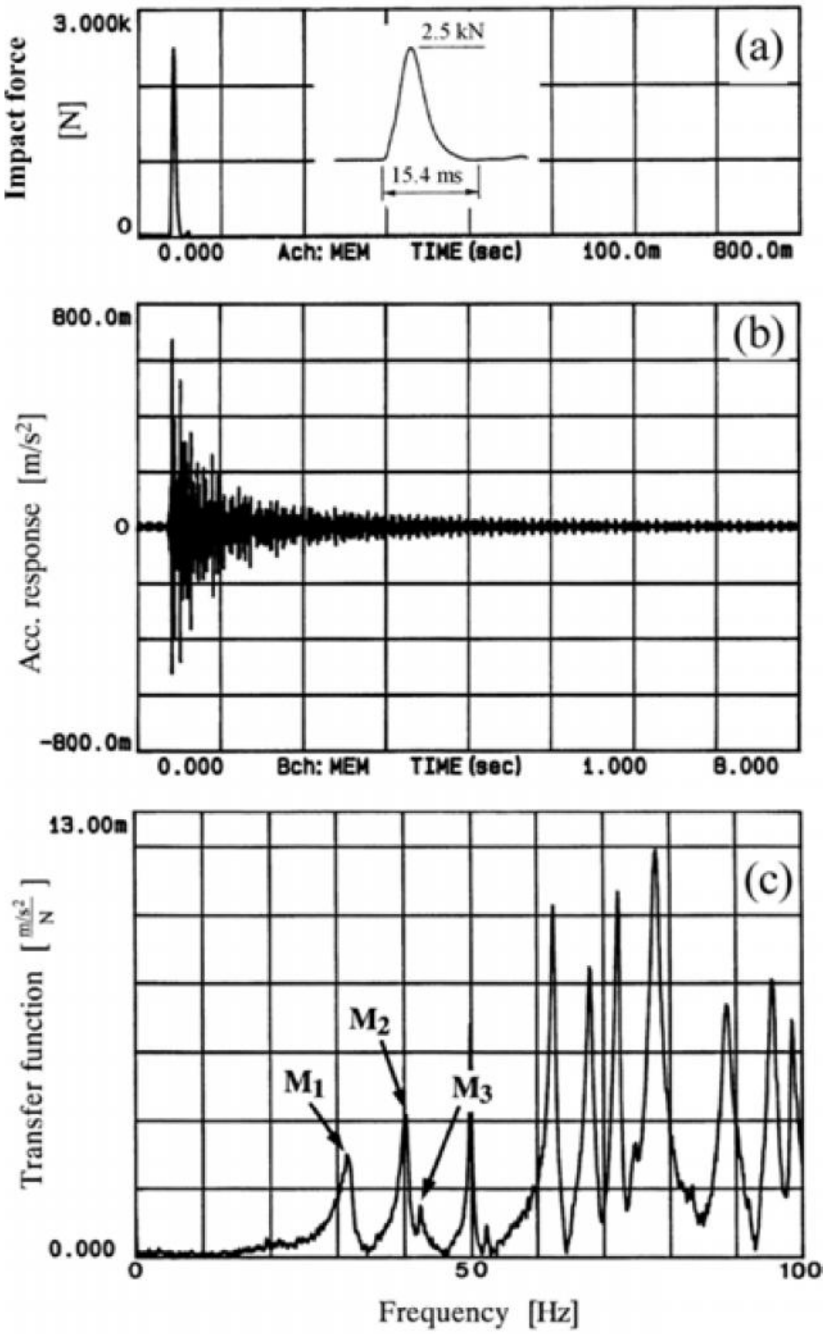

RESULTS AND DISCUSSION

In-Air Natural Vibration Characteristics

An overview of the frequency, the damping ratio and mode shape for these natural vibrations is shown in Table 1. The frequency of the fundamental mode is 30.5 Hz, and its mode shape suggests that it is essentially a uniform vibration across the entire span of the

Table 1: Experimental Modal Frequencies and Modal Damping Ratios from Experimental Modal Analysis of the Flap Gate

Mode Name	Frequency f_a[Hz]	Damping Ratio ¸ $_a$	Mode Shape
M_1	30.5	0.030	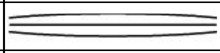
M_2	39.5	0.019	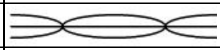
M_3	42.3	0.006	

Figure 4: Inverse Modal Indicator Function for the Flap Gate with the First Three Modal Frequencies Identified

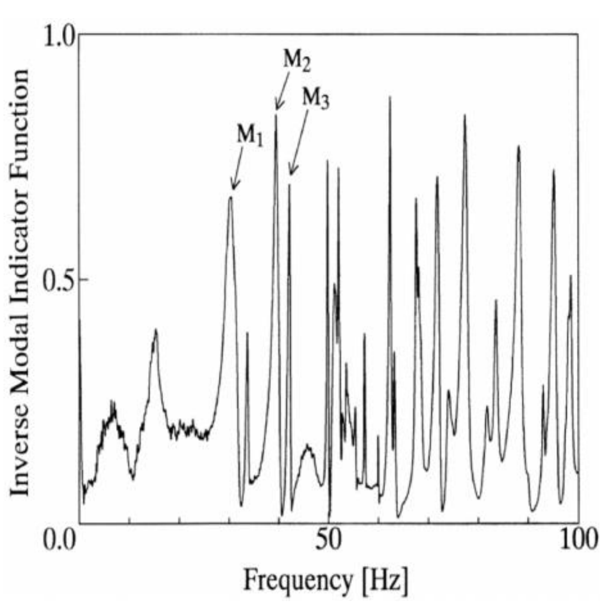

gate. A cross-sectional view of this fundamental mode is shown in Figure 5. This figure shows both the maximum upstream and downstream displacements of the skinplate. The numbers near the top of the gate and the letters on the right of the gate indicate the measurement locations given in Figure 2. From this mode chart, it is evident that the gate is undergoing rotational vibration. The small black circles show rough estimates of the centers of rotation on the left side of Figure 5. The bottom edge of the skinplate was taken as the zero reference location. The position of the center of rotation ranges from the center of the torque tube to its outer surface.

Self-Excited Vibration Characteristics of Flap Gate

The bottom of the skinplate was aligned with the upstream riverbed, as shown in Figure 1. The self-excited vibration tests were conducted with the upstream water depth maintained at 0.814 m. An acceleration waveform of the self-excited vibration with the gate at an inclination angle of 17.2º and an overflow depth of 16 mm (measured at Point 1A) is shown in Figure 6. The vibration grew rapidly and reached steady state after about 1 second. The excitation ratio ¶ was 0.0072, and the frequency f_w was 22 Hz.

Similar measurements were made for gate inclination angles from 15º to about 33º. The measured excitation ratios and frequencies at two locations are shown in Figure 7. Open circles represent the data from Points 1A, while the filled circles are for Point 12A.

The excitation ratio, shown in Figure 7, gradually decreases, as the gate inclination angle increases, because the overflow depth increases and the air cavity volume formed on the downstream side of the gate decreases. The frequency is locked onto a value of about 21.9 Hz for inclination angles less than about 22.2º. The frequency suddenly decreases to around 19.5 Hz once the inclination angle exceeds about 22.2º. With a continued increase in the inclination angle, the frequency gradually increases. The constant frequency at small inclination angles

Figure 5: Fundamental Mode of Natural Vibrations in Air Showing Modal Amplitude and Height of Rotational Center at Each Spanwise Measurement Location

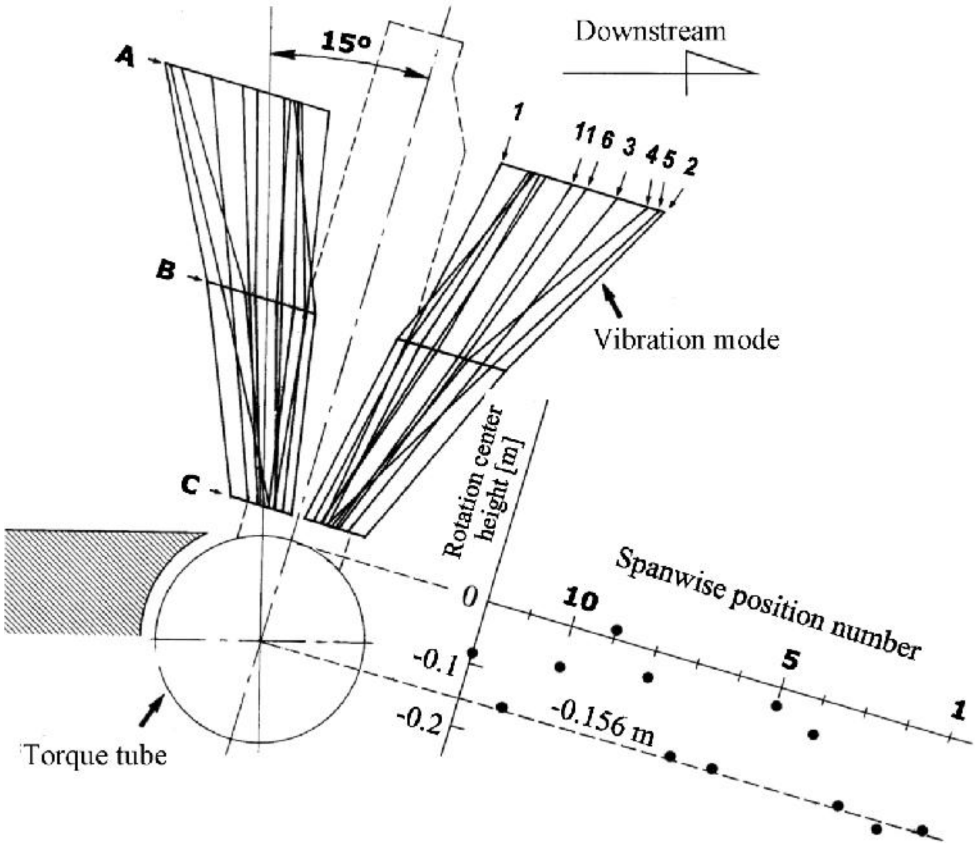

Figure 6: Waveform of Streamwise In-Water Acceleration for a Gate Inclination Angle of 17.2° and an Overflow Depth of 16 mm as Measured at Point 1A Showing Growth of Vibration

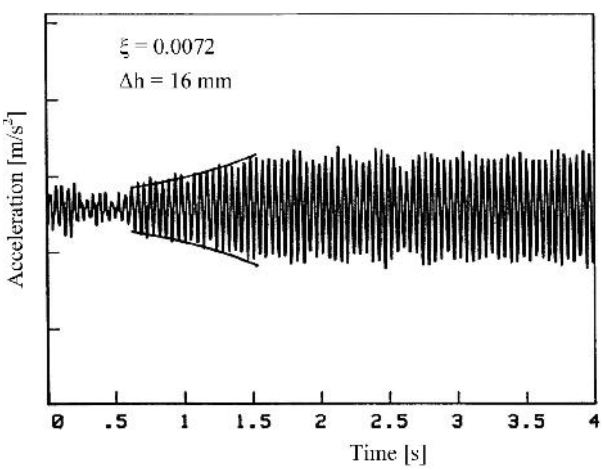

suggests a feedback mechanism related most likely to the oscillations of the nappe. The mechanism of the nappe oscillation is not the topic of this paper and is not examined further in this work.

Theoretical Calculations

Hydrodynamic Pressure

Analysis of the flow field is needed in order to calculate the hydrodynamic pressure. However, it is difficult to analyze exactly the flow field for the case in which the flap gate is inclined in the downstream direction. Therefore, the analysis will be confined to the simplified case in which the skinplate stands

Figure 7: In-Water Self-Excited Vibration Characterized by (a) Excitation Ratio, and (b) Vibration Frequency (Open Circles are for Point 1A; Filled Circles are for Point 12A)

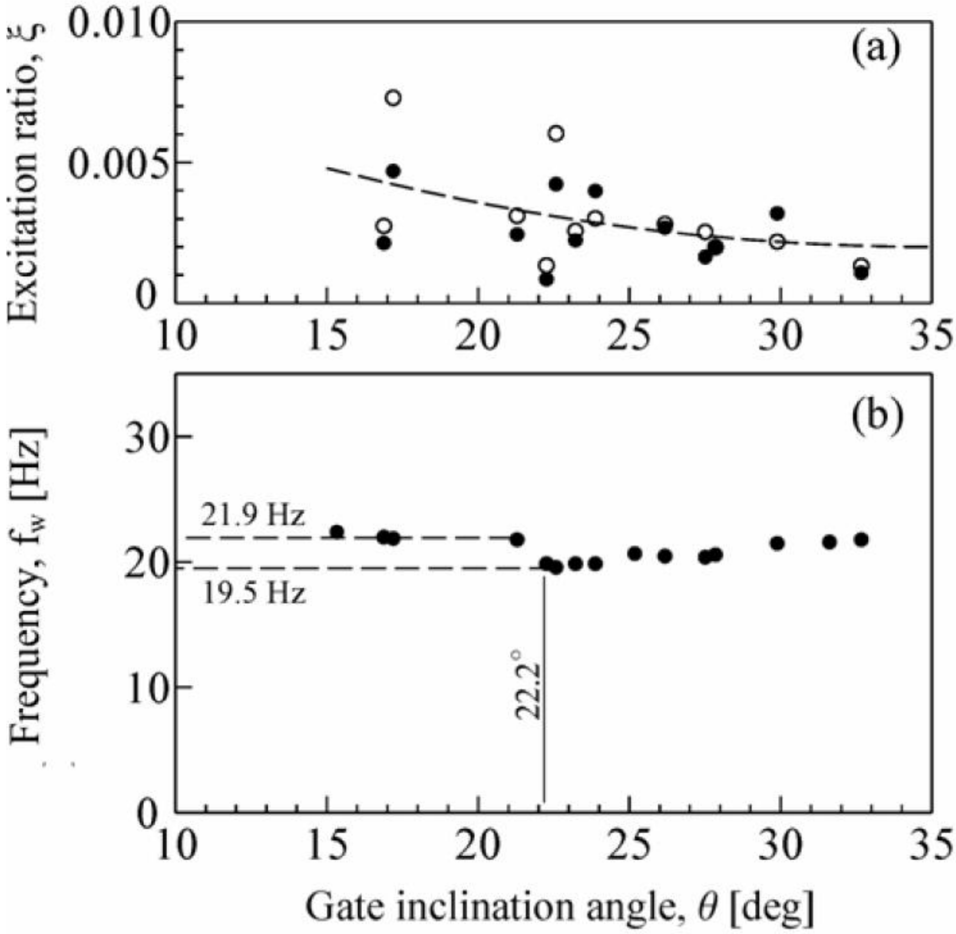

vertically and performs the rotational vibration with small amplitude, as shown in the left side of Figure 8. The dimensional coordinate Y is along the vertical skinplate and is defined as positive upward from the mean water surface, which corresponds to the dimensional coordinate X. The water depth of the upstream reservoir is represented by d_0. The top of the vertical skinplate above the riverbed is given as d_g; the height of the rotation center above the riverbed is given as R_s. As shown in Figure 8, the rotation center is lower than the upstream riverbed and R_s takes on a negative value.

The pressure change near the water surface is comparatively small. Therefore, the effect of the overflow water on the induced hydrodynamic pressure at larger depths is assumed to be insignificant. Instead, the overflow water depth was disregarded and it was replaced by a rigid wall vibrating with the vertical skinplate. The hydrodynamic pressure induced by the vertical skinplate vibration can be calculated by applying the potential-flow theory developed by Rayleigh (1945) and Lamb (1932) for dissipative wave-radiation problems. The validity of the analysis has been confirmed in model tests (Ishii, 1990, for

Figure 8: Vertical Weir-Plate Model on the Left, and Calculated Values of Vibration-Induced Hydrodynamic Pressure on the Right

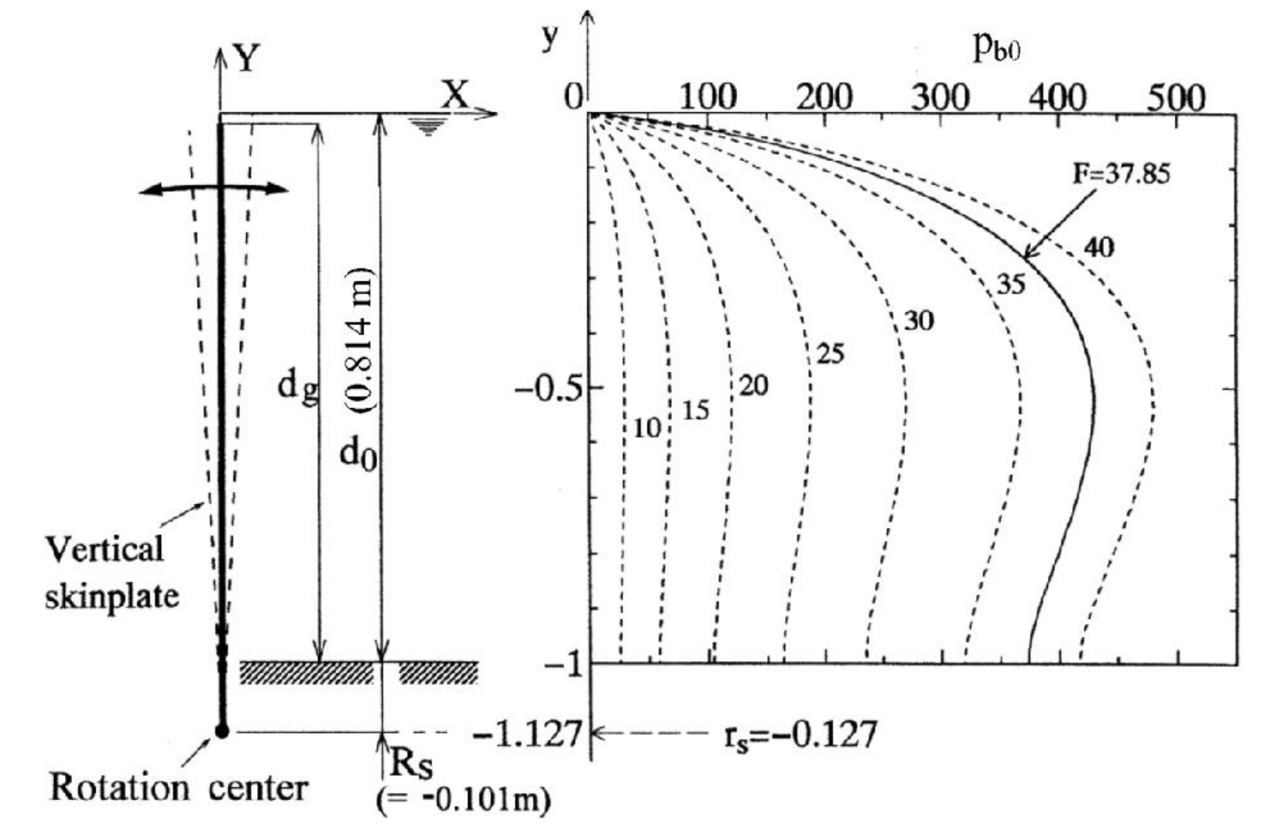

example). See the papers by Ishii and Imaichi (1977), Ishii (1990 and 1992), Ishii and Naudasher (1992), Anami and Ishii (1998a and 1998b) and Anami *et al.* (2012a and 2012b) for details of the theory.

The vertical axis y is the non-dimensional coordinate along the vertical skinplate:

$$y \equiv \frac{Y}{d_0} \qquad \text{...(2)}$$

Therefore, $y = -1$ corresponds to the upstream riverbed. The abscissa is the non-dimensional pressure amplitude, defined by the following expression:

$$p_{b0} \equiv \frac{P_{b0} / {}^{\circ}g}{(d_0 - R_S)\Psi_0} \qquad \text{...(3)}$$

where Ψ_0 is the amplitude of the rotation angle of the vertical skinplate. Thus, p_{b0} represents the ratio of the hydrodynamic pressure head corresponding to P_{b0} to the vibration amplitude at the top of the vertical skinplate.

An expression for hydrodynamic pressure induced by the rotational vibration of the vertical skinplate, P_b, from the previous study by Anami *et al.* (2012a), can be reduced to the non-dimensional pressure p_b acting on the vertical skinplate at $x = 0$. This non-dimensional pressure p_b is given by the following superposition of the acceleration and velocity terms:

$$p_b = p_{bs}\left(\frac{F_0}{F}\right)^2 \cdot \,'' + p_{bp}\left(\frac{F_0}{F}\right) \cdot \,' \qquad \text{...(4)}$$

where · represents the non-dimensional rotation angle and the prime represents the derivative relative to the non-dimensional time, *t*, given as follows:

$$\cdot \equiv \frac{\Psi}{\Psi_0} \quad \textit{and} \quad t \equiv \frac{T}{1/\Omega_a} \qquad \text{...(5)}$$

The Froude number *F* and the basic Froude number F_0 are defined by

$$F \equiv \sqrt{\frac{d_0}{g}}\,\Omega_w \quad \textit{and} \quad F_0 \equiv \sqrt{\frac{d_0}{g}}\,\Omega_a \qquad \text{...(6)}$$

where the in-water and in-air frequencies are represented by Ω_w and Ω_a, respectively. Therefore, the ratio of the two Froude numbers, F/F_0, represents the in-water to in-air frequency ratio:

$$\frac{F}{F_0} = \frac{\Omega_w}{\Omega_a} \quad \textit{or} \quad \frac{F}{F_0} = \frac{f_w}{f_a} \qquad \text{...(7)}$$

The variables p_{bs} and p_{bp} in Equation (4) are the non-dimensional pressure amplitudes of the so-called "standing and progressive pressure-wave components," respectively, which are given in the following series summations:

$$p_{bs}(x,y) = -\frac{2F^4}{1-r_s}\sum_{j=1}^{\infty}\left[\frac{1}{{*}\text{¦}_j^2}\left(r_s-\frac{1}{2}\right) + \frac{2}{\text{®}}\sum_{n=1}^{\infty}\frac{1}{n}\frac{1}{\text{¦}_j^2-\left(n\text{®}/\;{*}\right)^2} \times\left\{r_s \sin\frac{n\text{®}}{*} + \frac{*}{n\text{®}}\left(\cos\frac{n\text{®}}{*}-1\right)\right\}\right] \times\frac{\cos\text{¦}_j\left(y+{*}\right)}{\cos\text{¦}_j\,{*}}\frac{1}{W'\left(i\text{¦}_j\right)/i} \qquad \text{...(8)}$$

$$p_{bp}(x,y) = \frac{2F^4}{1-r_s}\left[\frac{1}{{*}\P_0^2}\left(r_s-\frac{1}{2}\right) + \frac{2}{\text{®}}\sum_{n=1}^{\infty}\frac{1}{n}\frac{1}{\P_0^2+\left(n\text{®}/\;{*}\right)^2} \times\left\{r_s \sin\frac{n\text{®}}{*} + \frac{*}{n\text{®}}\left(\cos\frac{n\text{®}}{*}-1\right)\right\}\right] \times\frac{\cos\P_0\left(y+{*}\right)}{\cos\P_0\,{*}}\frac{1}{W'\left(\P_0\right)} \qquad \text{...(9)}$$

in which r_s represents the reduced rotation center height, defined by

$$r_s \equiv \frac{R_S}{d_0} \qquad \text{...(10)}$$

which takes on a negative value in the present case. The value was assumed to be the average of the experimental values shown in Figure 5, which was 0.101 m, giving a non-dimensional average height of the rotation center of $r_s = -0.127$ which is also indicated in Figure 8.

The variables $\P_0$ and ¦_j (j = 1, 2, 3, …) in Equations (8) and (9) are the solutions of the following two transcendental equations:

$\P_0 \tanh\left(\P_0\;{*}\right) = F^2$ and $\text{¦}_j \tan\left(\text{¦}_j\;{*}\right) = -F^2$ (j = 1, 2, 3, ...) ...(11)

In addition, the functions $W'\left(i\text{¦}_j\right)/i$ and $W'\left(\P_0\right)$ included in Equations (8) and (9) are given, respectively, by the following two expressions:

$$W'\left(i\text{¦}_j\right)/i = \tan\text{¦}_j\;{*} + \frac{\text{¦}_j\;{*}}{\cos^2\text{¦}_j\;{*}}$$

and

$$W'\left(\P_0\right) = \tanh\P_0\;{*} + \frac{\P_0\;{*}}{\cosh^2\P_0\;{*}} \qquad \text{...(12)}$$

where * represents the ratio of the gate submergence depth d_0 to the upstream reservoir depth, which has been assumed to take on a value of 1.0 for the present case.

The resultant vector magnitude of hydrodynamic pressure $\left(p_{b0} \equiv \sqrt{p_{bp}^2 + p_{bs}^2}\right)$ of the standing and progressive pressure components can be calculated. The calculated amplitudes of the hydrodynamic pressure, p_{b0}, are shown in the right side of Figure 8 in terms of the Froude number, introduced in Equation (6). The Froude number represents the dynamic similarity of flow field and can also be written as follows:

$$F \equiv 2® f_w \times \sqrt{\frac{d_0}{g}} \qquad \text{...(13)}$$

Inserting the measured frequency of the self-excited vibrations, f_w, of about 20.9 Hz, as shown in Figure 7b, with the water depth d_0 of 0.814 m, yields a Froude number of 37.9 for the present tests. The non-dimensional pressure amplitude distribution for this Froude number is shown by the solid line in Figure 8. As previously mentioned, in these calculations the skinplate rotation center height R_s was assumed to take on the mean experimental value of –0.101 m, with a corresponding value of r_s = –0.127 (rounded to –0.13 in subsequent calculations).

The hydrodynamic pressure attains its maximum value of about 430 (corresponding to 0.43 m of water) near the center of the vertical skinplate when the top of the vertical skinplate vibrates with an amplitude of merely 1 mm.

Added Mass and Frequency Ratio

The water added moment of inertia, ΔI, can be calculated by integrating the hydrodynamic pressure moment around the rotation center over the vertical skinplate. As a result, one may introduce the non-dimensional added mass $\Delta m_{.}$, defined by

$$\Delta m_{.} \equiv \frac{\Delta I/(d_0 - R_S)^2}{°d_0^2 W_0} \qquad \text{...(14)}$$

The added moment of inertia was divided by the square of the rotation radius (d_0-R_S), to convert it into the equivalent mass. W_0 is the gate span of 14.8 m. The denominator is the representative water mass contained in the volume of $d_0^2 W_0$. The calculated results for the non-dimensional added mass as a function of the inclination angle are shown in Figure 9a, where the solid line is for the non-dimensional rotation center mean height of –0.13. In addition, the broken lines are for the r_s values of 0.0 and –0.19, which were the maximum and minimum values of the non-dimensional rotation center height r_s from the experimental data. An increase in the inclination angle is simulated by decreasing the height of the vertical skinplate top from the riverbed, d_g. As a result of this slight decrease in d_g, the added moment of inertia, ΔI, decreases slightly, with a corresponding slight decrease in the non-dimensional added mass.

The in-water frequency of the flap gate, f_w, is substantially reduced relative to its natural frequency in the air, f_{a1}, due to the added mass of the water. The ratio of these two frequencies can be calculated from the following expression (see Anami and Ishii, 1998a):

$$\frac{f_w}{f_{a1}} \equiv \frac{1}{\sqrt{1 + \sim_{.} \Delta m_{.}}} \qquad \text{...(15)}$$

where $\sim_{.}$ is the water to gate mass ratio, defined by

Figure 9: (a) Calculated Reduced Added Mass as a Function of Gate Inclination Angle, and (b) Computed (Lines) and Measured (Filled Circles) Frequency Ratio of In-Water Vibration to In-Air Vibration for the Same Range of Gate Inclinations

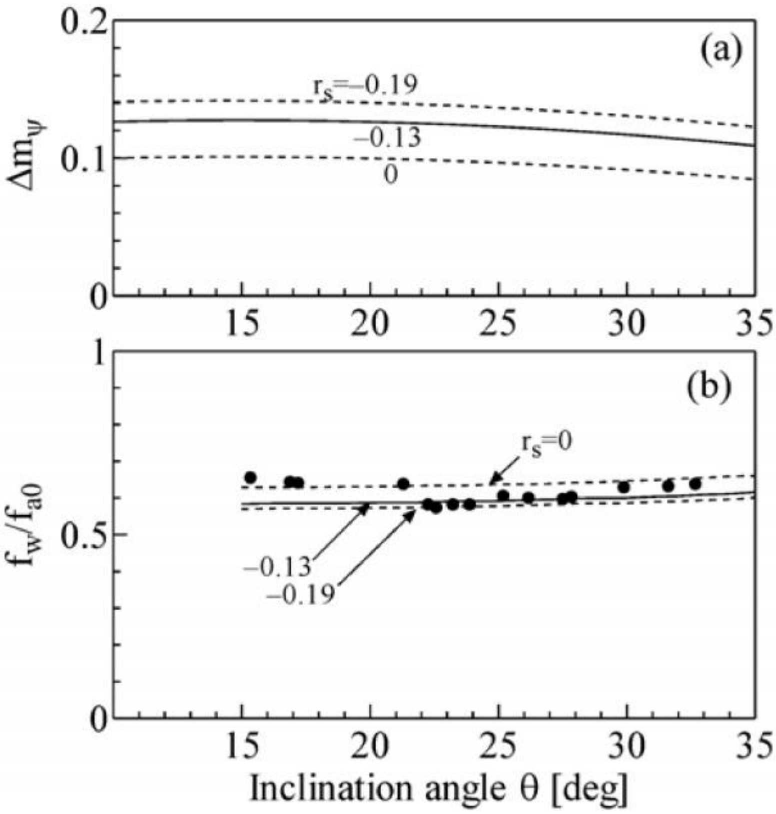

$$\tilde{\ }_{.} \equiv \frac{°d_0^2 W_0}{I_{.}/(d_0 - R_S)^2} \quad ...(16)$$

The numerator in the above expression is the representative water mass and the denominator is the equivalent vertical skinplate mass which can be calculated by dividing the moment of inertia of the vertical skinplate, $I_{.}$, by the square of the rotation radius $(d_0 - R_s)^2$. The moment of inertia, $I_{.}$, for the present flap gate took on a value of 545.8 kg × m^2, resulting in a mass ratio of 15.1. The solid line (for r_s = –0.13) and broken lines (for r_s = 0 and –0.19) in Figure 9b show the calculated results for the frequency ratio. As the inclination angle increases, the frequency ratio shows a slight increasing tendency, caused by a slight decrease in the non-dimensional added mass.

Unfortunately, the spoilers shown in Figure 2 were still attached when the in-air vibration tests were made. Subsequently they were removed for the in-water self-excited vibration tests. The measured in-air natural frequency of 30.5 Hz for the fundamental mode, shown in Table 1, was scaled to 34.1 Hz for the flap gate without spoilers. Dividing the measured frequency data shown in Figure 7b by the corrected in-air natural frequency, the measured frequency ratio data are obtained, as shown in Figure 9b. It is evident that the theoretical calculations accurately reflect the measured data.

CONCLUSION

The analytical method for calculating the hydrodynamic pressure exerted on vibrating gates, based on the potential flow theory for the dissipative wave radiation problems, has been previously validated on various types of laboratory-scale model gate test. In the present set of experiments, the analytical method was indirectly validated for a full-scale gate by using the measured frequency data for the self-excited vibrations of the flap gate installed in a river in Japan. Thus, it appears reasonable to expect that using the same analytical method, predictions of the in-water vibration frequency and the induced hydrodynamic force are possible for flap gates as well as for other types of gates, such as Tainter gates and long-span gates, in full-scale applications.

ACKNOWLEDGMENT

The authors wish to acknowledge financial support provided by a Science and Research Grant from the Japanese Ministry of Education. The authors also wish to acknowledge the cooperation and assistance of the village office of the village of Soni in the Nara Prefecture in carrying out these field studies. The authors extend their special thanks to Mr. Keiji Sakamoto, Dr. Akinori Nakata, Mr. Takuya Tanaka, and Mr. Takumi Tachibana, for their assistance in conducting the field impact tests and in the subsequent computer calculations for the modal analysis.

REFERENCES

1. Anami K and Ishii N (1998a), "In-Water Streamwise Vibration of Folsom Dam Radial Gates in California", Proceedings of 1998 ASME Pressure Vessels and Piping Conf., Vol. 363, pp. 87-93, San Diego, USA.
2. Anami K and Ishii N (1998b), "In-Air and In-Water Natural Vibrations of Folsom Dam Radial Gate in California", Proceedings of 11th International Conference on Experimental Mechanics, Experimental Mechanics 1, Allison (Ed.), pp. 29-34, Balkema, Rotterdam, Oxford, UK.
3. Anami K and Ishii N (1999), "Flow-Induced Coupled-Mode-Vibration of Folsom Dam Tainter-Gates in California", Proc. of 1999 ASME Pressure Vessels and Piping Conf., Vol. 396, pp. 343-350, Boston, USA.
4. Anami K and Ishii N (2000), "Flow-Induced Dynamic Instability Closely Related to Folsom Dam Tainter-Gate Failure in California", in Ziada S and Staubli T (Eds.), *Flow-Induced Vibration*, pp. 205-212, Balkema, Rotterdam.
5. Anami K and Ishii N (2003), "Model Tests for Non-Eccentricity Dynamic Instability Closely Related to Folsom Dam Tainter-Gate Failure", Proc. of ASME Pressure Vessels and Piping Conference, Vol. 465, pp. 213-221, Ohio, USA.
6. Anami K, Ishii N and Knisely C W (2012a), "Pressure Induced by Vertical Planar and Inclined Curved Weir-Plates Undergoing Streamwise Rotational Vibration", *Journal of Fluids and Structures*, Vol. 29, pp. 35-49.
7. Anami K, Ishii N and Knisely C W (2012b), "Added Mass and Wave Radiation Damping for Flow-Induced Rotational

Vibrations of Skinplates of Hydraulic Gates", *Journal of Fluids and Structures*, Vol. 35, pp. 213-228.

8. Anami K, Ishii N, Knisely C W and Matsumoto Y (2000), "Measured and Calculated Vibration Characteristics of a Full-Scale Flap Gate Undergoing Self-Excited Vibration", Vol. 414, No. 1, pp. 23-30, ASME-Publications-PVP.
9. Ishii N (1990), "Flow-Induced Vibration of Long-Span Gates (Verification of Added Mass and Fluid Damping)", *JSME International Journal*, Series II (Fluid Engineering, Hear Transfer, Power, Combustion, and Thermophysical Properties), Vol. 33, pp. 642-648.
10. Ishii N (1992), "Flow-Induced Vibration of Long-Span Gates (Part I: Model Development)", *Journal of Fluids and Structures*, Vol. 6, pp. 539-562.
11. Ishii N (1995a), "Folsom Dam Gate Failure Evaluation and Suggestions", Report Submitted to US Bureau of Reclamation, August 24.
12. Ishii N (1995b), "Folsom Dam Gate Failure Evaluation Based on Modal Analysis and Suggestion", Report Submitted to US Bureau of Reclamation, November 8.
13. Ishii N (1997), "Dynamic Stability Evaluation for Folsom Dam Radial Gate and Its Inherent Non-Eccentricity Instability", Report Submitted to US Bureau of Reclamation, July 17.
14. Ishii N and Imaichi K (1977), "Water Waves and Structural Loads Caused by a Periodic Change of Discharge from a Sluice Gates", *Bulletin of the Japan Society of Mechanical Engineers*, Vol. 20, No. 6, pp. 998-1007.
15. Ishii N and Naudascher E (1992), "A Design Criterion for Dynamic Stability of Tainter Gates", *Journal of Fluids and Structures*, Vol. 6, pp. 67-84.
16. Lamb H (1932), "Hydrodynamics", pp. 398-403, Cambridge University Press.
17. Rayleigh J W S (1945), "The Theory of Sound", Vol. 2, pp. 4-8, Dover, New York.

APPENDIX

Nomenclature

d_0	water depth of the upstream
d_g	distance to the skinplate top from the river bed
F	Froude number
f_{a1}	in-air vibration frequency
f_w	self-excited vibration frequency
g	gravity acceleration (m/s^2)
I_ψ	moment of inertia of skinplate around its rotation center
P_b	hydrodynamic pressure
p_b	reduced hydrodynamic pressure
R_s	skinplate rotation center height
r_s	non-dimensional rotation center height
T_i	transfer function
W_0	spanwise length of the skinplate (m)
Y	coordinate along the skinplate
y	non-dimensional coordinate along the skinplate
~ .	water-to-gate mass ratio,
ΔI	additional moment of inertia
Δm .	reduced added mass
–	gate inclination angle
¶	excitation ratio
°	density of water (kg/m^3)
¤	phase-lag
Ψ_0	amplitude of skinplate